Chapter 4

Soft X-Ray Scattering Apparatus

Within the framework of this thesis, a new scattering apparatus was built. The result is a state-of-the-art soft x-ray diffractometer, which was successfully used not only for this work, but also by a number of collaborators to study a variety of physical phenomena and samples, ranging from charge- and orbital-ordering effects in transition-metal oxides to magnetic properties of ultra-thin films and nano-dot arrays. In the following, this versatile ultrahigh-vacuum compatible two-circle diffractometer for soft x-ray scattering is described.

From a technical point of view, scattering experiments with soft x rays are rather demanding, since the strong absorption of soft x rays in air requires a diffractometer working at least in high vacuum. Furthermore, the technique is rather surface sensitive due to the enhanced x-ray absorption at resonance, which may require in-situ sample preparation. Also, experiments at cryogenic temperatures can suffer from residual gas adsorption, which can substantially influence reflectivity measurements. Therefore, ultrahigh-vacuum (UHV) conditions are favorable in many cases. The enormous potential of resonant soft x-ray scattering has led to the development of suitable diffractometers at synchrotron radiation facilities [117–121]. Common to the design of these diffractometers is a detector mounted on an arm that is moved through the vacuum tank. Thus, the detector moves with respect to all flanges of the vacuum chamber, which restricts electrical and mechanical access. In order to expand the field of application of this technique, it is desirable and to some extent even crucial, to apply complex detectors like an energy or polarization analyzer [122] or a position-sensitive detector.

The present apparatus was designed to enable true UHV conditions in combination with versatile mounting of detectors and mechanics. It avoids complex electrical connections and in-vacuum motors and works at pressures down to 10^{-11} mbar. With a suitable cryostat, effective sample cooling can be obtained, making experiments at least down to 5 K feasible. The apparatus has a compact design, leaving the region around the sample free to accommodate further instrumentation like magnets etc. Further degrees of freedom for sample movement can be readily implemented. The following sections present the design of its essential part, a compact two-circle diffractometer, and the vacuum chamber.

4.1 Diffractometer

The independent rotation of a sample and a detector by means of a two-circle diffractometer requires two concentric rotational degrees of freedom. This is typically achieved by the use of two conventional rotary feedthroughs, either mounted on top of each other or on opposite sides of the vacuum chamber. High mechanical precision in combination with a compact design and high flexibility is achieved in our setup by a novel differentially pumped two-stage rotary feedthrough [123]. It is made from

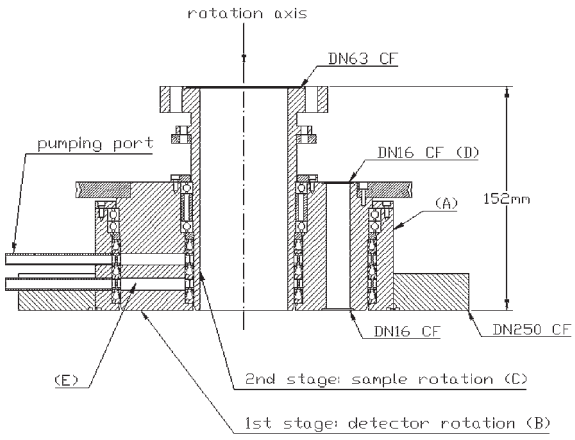

Figure 4.1: *Schematic drawing of the two-stage rotary feedthrough used as two-circle diffractometer in the present setup.*

stainless steel and consists essentially of three parts, as depicted in Fig. 4.1: The outer part is a tube (A) welded to a DN250 CF UHV flange. A disc of 165 mm outer diameter (B) acts as a shaft for the rotation of the detector. This part is equipped with six bores (D) parallel to the axis of rotation, which can be used for electrical and mechanical connections to the detector. The bores have DN16 CF flanges both at the atmospheric and the vacuum side, permitting to mount parts outside as well as inside the chamber. These flanges are used to install and connect the detectors which avoids cables moving inside the vacuum. For the sample rotation, a second tube shaft (C) with DN63 CF flange is mounted concentric to the detector rotation. This shaft leaves the axis of rotation free for versatile sample mounting, like, e.g. , directly on a cryostat for effective cooling. With this design, the full angular range of +/- 180° for the sample rotation (ω) is available, and about +/- 170° for the detector rotation (2Θ), limited only by the size of the detector. The sealings of the two rotations include differential pumping in two stages, which is realized by a single pair of pumping ports. They are connected to the sealings of the sample rotation by horizontal bore holes (E) in the detector shaft (B). The instrument is driven by stepper motors and worm gears outside the vacuum chamber. Control of the stepper-motor motion as well as data acquisition is performed by means of a Linux PC using standard SPEC software. The reproducibility of the angular positions was found to be better than 0.004°. The two rotational axes have an offset and a tilt of less than 50 μm and 0.01°, respectively. Hence, the construction readily provides the accuracy required in typical soft x-ray scattering experiments. A particular advantage of the system is the possibility to mount various detector systems that even can be used simultaneously.

4.2 Detectors

In the present stage of development, the diffractometer is equipped with a conventional Si photo diode and a novel rotatable position sensitive detector as shown in Fig. 4.2. For many purposes, the silicon photo diode with an active area of 10 x 10 mm^2 (coated with Al to minimize the influence of parasitic visible light) was found to be sufficiently sensitive. The angular resolution can be adapted to the requirements of the experiment by a set of rectangular slits mounted on a carousel in front of the diode (Fig. 4.2(b)). The slits with sizes between 50 μm and 2 mm can be changed in situ and provide angular acceptances between 0.02° and 0.8°. The photo current is measured by a Keithley 6514

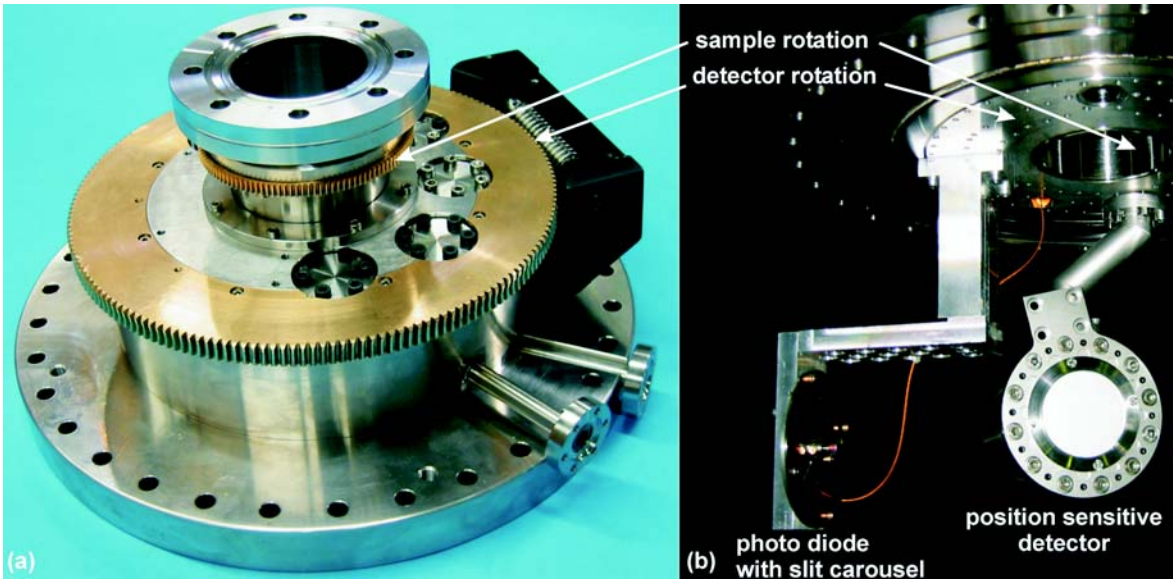

Figure 4.2: *Photograph of the diffractometer sketched in Fig. 4.1 (a) Atmospheric side of the diffractometer with mounted gear box for the detector rotation, without stepper motors. (b) vacuum-side with mounted photo-diode detector including a slit carousel and position sensitive phosphor-screen detector.*

Electrometer. Typical values at an undulator beamline at BESSY II can be as high as 50 μA in the direct photon beam (at $h\nu = 1100$ eV). The dark current of the diode limits the minimum detectable signal to approximately 0.1 pA. With a quantum efficiency of about 300 electrons per photon at this energy, these currents correspond to 10^{12} photons per second as a typical flux of the beamline and a minimum detectable scattering signal of about $2\text{x}10^3$ photons per second, i.e. , a dynamic range of about nine orders of magnitude. While this detector is well suited for many applications, the diffractometer design leaves enough flexibility to easily install more sensitive detectors involving avalanche photo diodes or channeltrons. For more complex diffraction patterns, a position-sensitive detector system was implemented into the system (right side of Fig. 4.2). It consists of a fluorescence screen and a CCD camera. The screen coated with P43 phosphor is placed in vacuum and converts soft x rays into visible light. The screen is read out by a small CCD-camera placed inside a small stainless steel tube, which itself is attached to one of the inside CF flanges on the detector circle (cf. Fig. 4.1 D, also visible in the right side of Fig. 4.2 b). The camera is sealed from the vacuum by a glass window (behind the fluorescence screen) that allows to detect the visible light. Hence, the camera itself remains in ambient atmosphere and the cable connections can be made without passing the vacuum. Yet, the position-sensitive detector can be rotated inside the chamber. Such a two-dimensional detector is essential for the study of laterally structured materials. As an example, the diffraction pattern of a square lattice of CoPt multilayer dots is shown in Fig. 4.3, recorded with a photon energy corresponding to the Co L_3 resonance ($h\nu = 779$ eV). The horizontal direction in this figure corresponds to different 2Θ angles, while the vertical direction represents the angle with respect to the horizontal scattering plane. With this detector, two-dimensional diffraction patterns can be readily recorded, while the diode detector would average along the vertical direction over a few diffraction spots, yielding information that would be difficult to interpret in terms of peak widths and distances. In order to test the performance of the position-sensitive detector, a comparison to the diode detector was made. For this purpose, a nanostructered sample consisting of CoPt multilayer stripes was used. The sample was mounted with the stripes in the vertical direction, resulting in a single

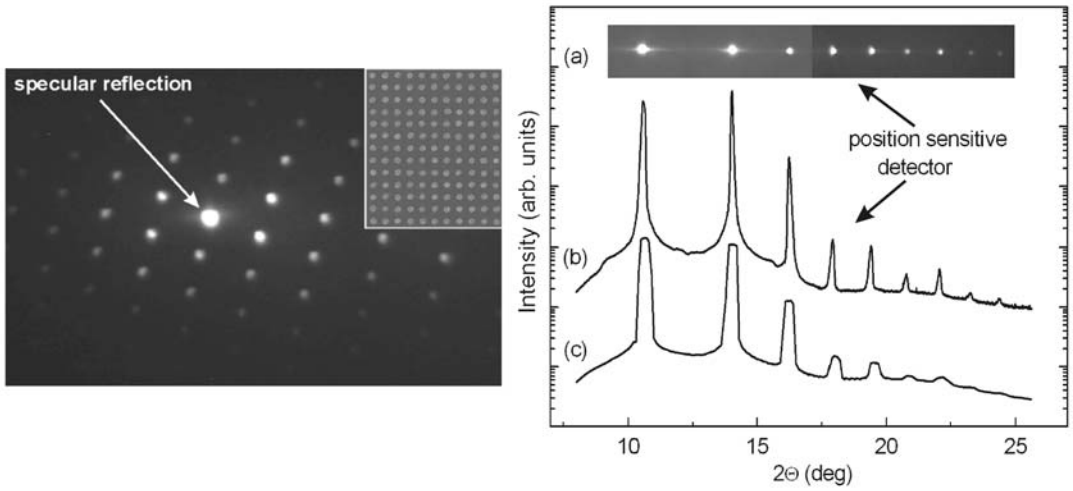

Figure 4.3: *Left: Two-dimensional diffraction pattern from a square lattice arrangement of CoPt-nanodots with a dot distance of approximately 150 nm, recorded at the Co-L_3 edge. The inset shows a scanning electron micrograph of a comparable sample taken from Ref. [124]. Right: (a) Two-dimensional diffraction pattern from a stripe array of CoPt multilayers with a spacing of approximately 280 nm, recorded at the Co-L_3 edge. (b) Corresponding line scan. (c) Detector scan recorded with the Si diode.*

horizontal line of diffraction spots that can be recorded by both, the photo diode and the position sensitive detector. Figure 4.3 (a) displays the two-dimensional diffraction pattern obtained from this structure using a photon energy corresponding to the Co L_3 edge. From this pattern, a line profile in the horizontal direction was extracted, which represents a detector scan (2Θ) after proper calculation of the scattering angle from the position on the detector. The results are shown in Fig. 4.3 (b), which can be compared with the corresponding scan with the diode detector (Fig. 4.3 (c)). In the latter case, the 1 mm slit had to be used due to low count rates, resulting in poor resolution compared to the width of the diffraction structures. The shape of the peaks in Fig. 4.3 (c) is determined by the rectangular slit function rather than the diffraction features. Besides this resolution effect, however, the two curves are essentially the same, proving an excellent performance of the position-sensitive detector. Notably, the latter even outperforms the Si diode in terms of sensitivity at least for the photon energy of the Co L_3 resonance. While the scan using the diode took about 10 minutes, the position sensitive detector recorded the pictures in less than 30 seconds with a ten times higher point density. Furthermore, the angular resolution is better by a factor of two, even if the diode is used with the smallest slit (50 μm).

4.3 Vacuum Chamber and Vacuum Conditions

The x-ray diffraction setup combines the requirements of high precision and novel types of detectors with true UHV-conditions. This aim was already taken into account in the design and fabrication of the diffractometer and vacuum chamber: The novel rotary feedthrough minimizes the necessary in-vacuum constructions which is one of the keys to reach pressures well below 10^{-9} mbar. The diffractometer is mounted on top of a cylindrical vacuum chamber permitting a horizontal scattering geometry. The chamber (displayed in Fig. 4.4) with an inner diameter of 400 mm and a height of 300 mm is equipped with twelve DN63 CF flanges in the scattering plane for windows and further instrumentation, such as evaporation sources, sputter gun, or a setup to measure magnetooptical Kerr effect. In a second plane, 150 mm below the scattering plane, two DN150 CF flanges are available for

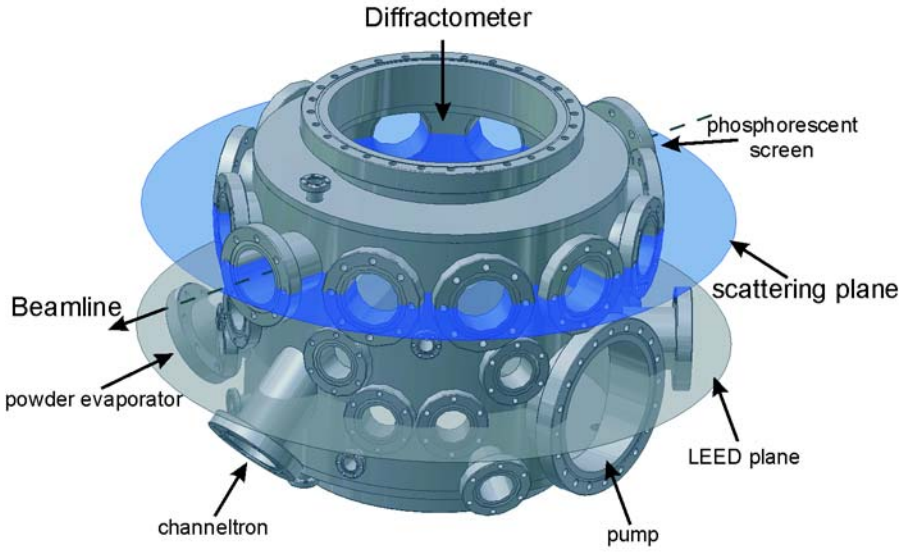

Figure 4.4: *Volume model of the vacuum chamber. The diffractometer is mounted on the top DN250 CF flange.*

mounting the main pump and a LEED apparatus. Further DN63 CF and DN38 CF flanges are included in this plane. In order to optimize the vacuum conditions, the effective surface of the chamber was reduced by means of electro-polishing. The entire chamber is pumped by a Pfeiffer TMU 521P turbomolecular pump (500 l/s) backed by a Pfeiffer turbomolecular pumping station consisting of a smaller turbomolecular pump and a membrane pre-vacuum pump. The latter station is also used for differential pumping of the rotary feedthrough of the diffractometer. Pre-vacuum pressure is monitored by a wide-range cold-cathode pressure gauge, while for the chamber three different pressure gauges are available: A Leybold extractor pressure gauge serves as the most precise pressure monitor. During the measurements, however, only a cold-cathode gauge can be used to avoid interfering visible light. In addition, a mass spectrometer permits to analyze the composition of the residual gas and to perform helium leak tests. Even without additional pumps, a base pressure of less than $1 \cdot 10^{-9}$ mbar can be readily achieved. Further improvement of the vacuum utilizes a combined cryogenic and sublimation pump mounted to the bottom DN250 CF flange displayed in Fig. 4.5. It is essentially a ring-shaped liquid nitrogen (LN_2) tank made of stainless steel with a capacity of about 3.5 liters of liquid nitrogen. The refill period of the tank of about 10 hours prevents a warm-up and subsequent pressure worsening during the break between two standard shifts at BESSY II. The tank is attached to the outer walls only by three small tubes which are also used to fill the tank. Even without a bake-out, the chamber reaches the 10^{-9} mbar range within twelve hours. However, a soft bake-out at about 120°C for one day and subsequent use of the LN_2 trap and the sublimation pumps yields base pressures of the order of 10^{-11} mbar. The remaining residual gas consists mainly of hydrogen.

The cold trap leaves a central hole of 150 mm to mount further instrumentation from the bottom, i.e. opposite to the diffractometer, like magnets that can rotate synchronously with the sample. At present, a ring-shaped electromagnet with an iron yoke and a gap of 10 mm, a rotatable permanent magnet or a Helmholtz-like coil pair are available, providing magnetic fields up to 2000 Gauss. The chamber is connected to the beamline via a CF63/CF38 adapter flange, which includes an additional aperture system and a removable gold mesh. The precise alignment of all components is crucial for the performance of the instrument. A rack system enables a positioning of the diffractometer with an

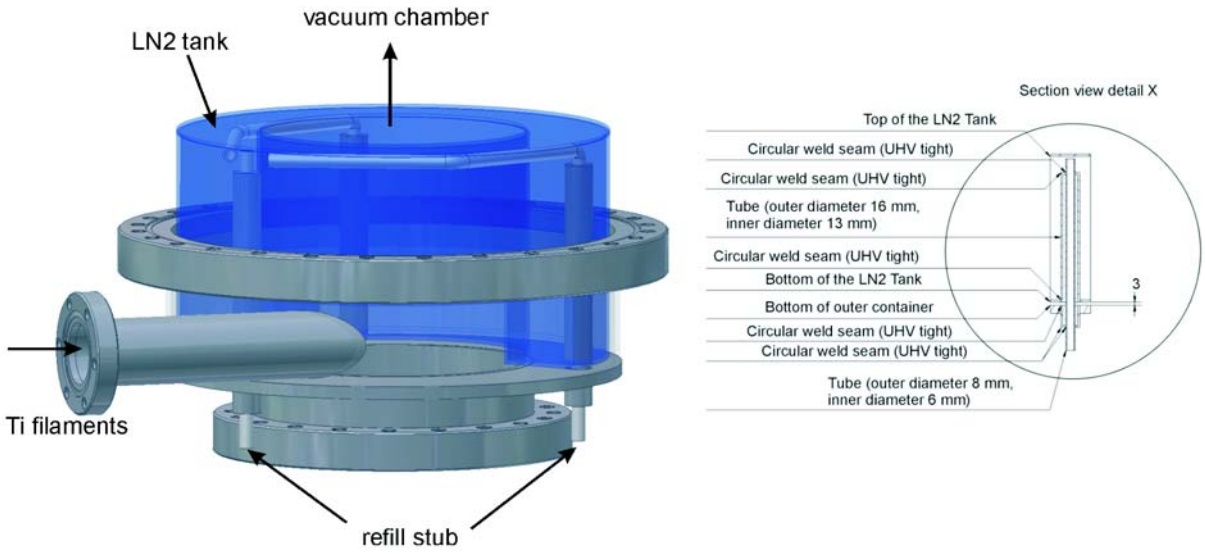

Figure 4.5: *Cold trap used in the scattering setup. Left: Volume model. The liquid nitrogen tank (blue) and the outer wall (gray) are displayed partly as transparent for clarity. Right: Cross-sectional drawing of the refill stubs.*

accuracy in the order of only a few μm. The whole setup is shown in figure 4.6.

4.4 Alignment Procedure

X-ray diffraction experiments require a high degree of accuracy concerning the alignment of the instrument. Ideally, the diffractometer axis of rotation lies in the center of the sample surface. For the necessary adjustments, the requirements concerning the accuracy are defined by the spot size of the x-ray beam which is typically of the order of 50 μm. In addition, in most cases, one would like to have the focus point of the beam to coincide with the sample surface. This minimizes the footprint effect[1] and the area over which the sample properties are averaged by the experiment. Both can become crucial in the case of small or rather inhomogeneous samples. The sufficient accuracy in this case is of the order of 1 mm due to small divergences at present beam lines of about 5 mrad. These requirements are realized by two separate manipulation systems. The sample can be moved with respect to the intersection point of the rotational axis and the scattering plane in three orthogonal directions by $\pm$10 mm with a custom-built xyz-table on top of the CF63-flange of the diffractometer with an accuracy of 10 μm for the horizontal shifts. An additional motorized 150 mm linear shift provides larger movements of the sample holder normal to the scattering plane with an accuracy of 20 μm. For the alignment of the diffractometer axis with respect to the beam, the chamber is mounted into a three-part rack system. The base consists of a frame resting on three stands that include the height adjustment. Beamline ports with heights between 1200 mm and 1650 mm are reachable without additional platforms. Above this lower frame, an aluminum table is mounted, which can be moved horizontally along the beam and in the perpendicular direction by spindle drives. The manipulations

[1] The decrease of scattered intensity, if the projected beam size exceeds the size of the sample surface.

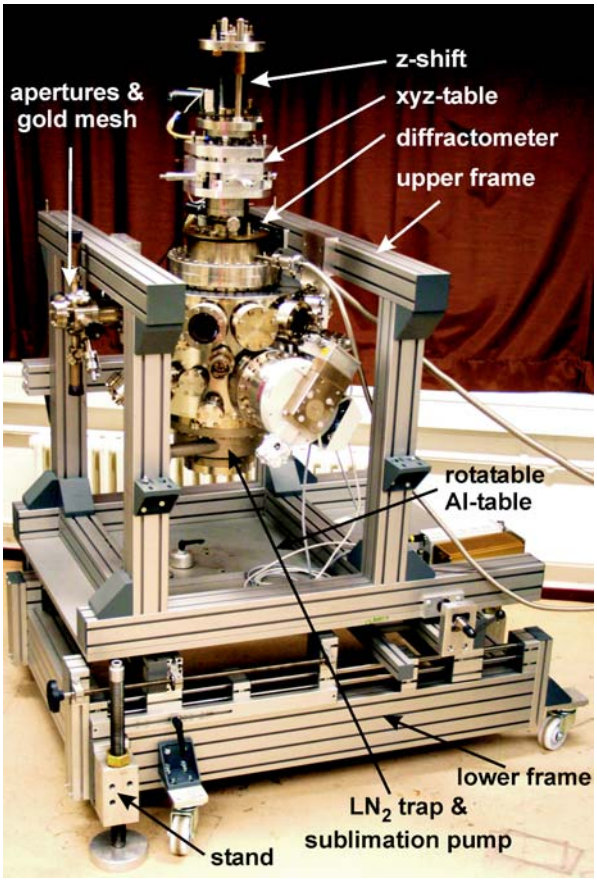

Figure 4.6: *Photograph of the complete diffractometer including the vacuum chamber and the rack.*

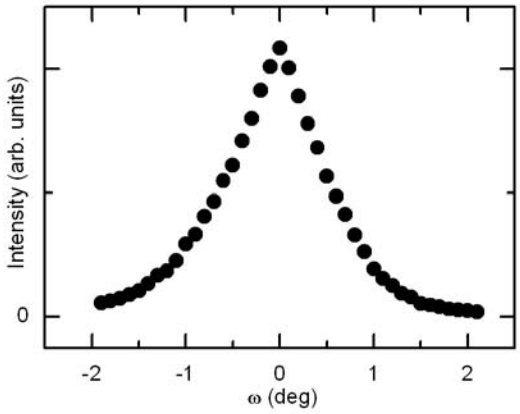

Figure 4.7: *Rocking scan at zero degree of a 20-ML thin EuTe sample. The essentially symmetric decrease of the intensity at both sides proves a properly aligned setup.*

are controlled by dial gauges mounted to the rack with an accuracy of the order of 10 μm. Directly on top of the lower table, a second table is mounted, which can be rotated around a vertical axis that is approximately aligned with the diffractometer axis. This second, rotatable table finally carries the vacuum chamber and the diffractometer. These translational degrees of freedom and the rotation permit an easy and straightforward alignment of instrument and sample: With the detector placed in the direct beam, the sample is manipulated by the xyz-table to cut the measured intensity in half. A subsequent rocking scan provides the information of the zero-position of the ω rotation (maximum of the scan) and the deviation of the sample position from the rotational axis in the direction parallel to the beam (symmetry of the scan). A properly-aligned setup is characterized by a maximum intensity at $\omega = 0^\circ$ with a symmetric decrease of the intensity on both sides as shown in Fig. 4.7. The deviation of the diffractometer axis normal to the beam is quantified by rotating the sample by 180°, starting from $2\Theta = \omega = 0$ with the intensity cut in half by the sample surface. Only for a precise coincidence of the rotational axis and the beam the sample shadows again half of the full beam intensity after the rotation. An observed deviation can be adjusted by a horizontal shift of the entire instrument by means of the rack system. A properly-aligned setup shows a symmetric rocking scan at zero degree and equal intensities for the $\omega = 0^\circ$ and $\omega = 180^\circ$ position.

4.5 Characterization of the Instrument

X-ray diffraction experiments measure the **Q**-dependence of the scattered intensity. The quality of the results strongly depends on the angular accuracy. The minimum required angular resolution is given by typical peak widths, which consequently also identifies the required angular accuracy of the instrument. While x-ray diffraction in the hard x-ray regime demands an accuracy of a few millidegrees, the required angular resolution in the soft x-ray range is typically not as high due to the smaller k-values, but still of the order of a few hundredth of a degree. The angular acceptance of the present instrument can be varied by different rectangular slits in front of the photo diode from $\pm 0.01^\circ$ to $\pm 0.4^\circ$, which matches the possible minimum angular resolution as a consequence of the beam divergence. Therefore, the same angular resolution and accuracy is required for the rotations of the diffractometer.

The instrument was carefully characterized after its completion. The relative orientation of the

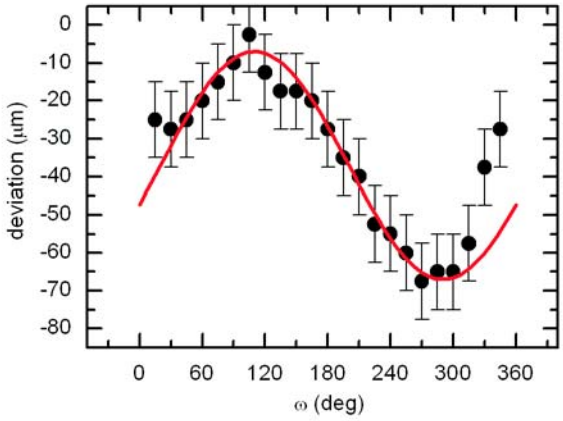

Figure 4.8: *Horizontal deviation of the measured position of a stainless steel tube on top of the diffractometer during a 2Θ rotation which was aligned in such a way that essentially no deviation during an ω rotation occurs. The red line corresponds to the expected behavior for an horizontal offset of both axes of 30 μm.*

two axes was tested in the following way: On top of the xyz-table, a steel tube was mounted. Its relative horizontal position with respect to the instruments frame was measured by several dial gauges (accuracy: 10 μm) mounted radial to the tube. The xyz-table was used to position the tube in the rotational axis of the ω rotation such that the dial gauges show a minimum change during a 360° rotation of ω caused by a small asymmetry of the tube. The additional deviation shown in Fig. 4.8 measured by a subsequent rotation of the 2Θ axis by 360°, is caused by a misalignment of the ω and 2Θ axes. This can be either a tilt or an offset, more probably both. The characterization yielded an upper limit for the offset and tilt of the axes (see Fig. 4.8) to be less than 50 μm or 0.01°, respectively.

The angular accuracy was checked by means of a laser mounted on top of the diffractometer. From the deviation of the laser spot position on a wall of 8 m distance, after multiple rotations by 360° as well as -360°, an angular accuracy of better than 0.004° was found for both rotational degrees of freedom, which readily fulfills the above-mentioned requirements.

This procedure does not ensure the same accuracy concerning the absolute angular position, for it contains no information on the regularity of a 360° rotation. That question is of importance in the case of scans realized by a combined angular motion of both rotational axes, like the $\Theta/2\Theta$-scans. Therefore, each time a longitudinal scan was used, rocking scans at different detector positions were performed as shown in Fig. 4.9. As can be seen, at both 2Θ positions the rocks are sufficient centered in order to measure the maximum reflected intensity. However, both peaks are not exactly centered at the $\Delta\omega = 0°$ position, displaced by 0.03°. While this finding can be caused by several influences, the number is an upper limit for the inaccuracy of the combined angular motion, which is well within the tolerances outlined before.

This last section described a diffractometer for soft x-ray scattering. With the novel diffractometer design all movements of sample and detector are included in a single rotary feedthrough, with the stepper motors outside the vacuum. Electrical contacts and mechanical feedthroughs to operate complicated detector systems can be mounted directly on the main feedthrough, avoiding complex in-vacuum constructions. Due to the excellent vacuum conditions this instrument is particularly suited for surface-sensitive experiments including in-situ film growth. The instrument can accommodate various sample holders such as cryostats for low-temperature experiments. The main features of the setup are:

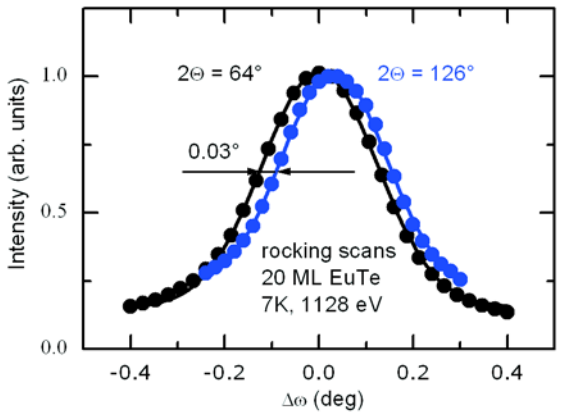

Figure 4.9: *Rocking scans at different detector positions (2Θ). $\Delta\omega$=0 corresponds to the expected position of maximum intensity $\omega = \Theta$.*

- base pressure < $1 \cdot 10^{-10}$ mbar
- low achievable sample temperature < 5 K (depending on the cryostat)
- nearly full 360°- angular range available for sample and detector
- angular accuracy < 0.004°
- alignment accuracy 10 μm

While the scattering apparatus performs already very well, further improvements are on the way concerning more sensitive detectors and higher magnetic fields. The design of the diffractometer feedthrough can be scaled to larger dimensions, providing larger bores (D) (Fig. 4.1) for instrumentation. These will offer even easier and more flexible mounting of complex detection systems and mechanics to drive, e.g. , polarization or energy analyzers. The setup was used at several beamlines at BESSY II, U49/2-PGM-1, UE56/2-PGM-2, UE56/1-PGM-b, U125/2-SGM and UE52-SGM, as well as at the UE46/1-PGM-1 beamline operated by the Hahn-Meitner institute proving an excellent performance. From the variety of performed experiments the last part of this thesis presents studies of ultra-thin AFM films of metallic holmium and semiconducting EuTe. The following chapter introduces the studied samples, their preparation as well as the sample holders.